RETRACTED: Surgical Treatments for Canine Anterior Cruciate Ligament Rupture: Assessing Functional Recovery Through Multibody Comparative Analysis

Giovanni Putame[1]*, Mara Terzini[1], Cristina Bignardi[1], Brian Beale[2], Don Hulse[3], Elisabetta Zanetti[4] and Alberto Audenino[1]

[1] Polito[BIO]Med Lab, Department of Mechanical and Aerospace Engineering, Politecnico di Torino, Turin, Italy, [2] Gulf Coast Veterinary Specialists, Houston, TX, United States, [3] Austin Veterinary Emergency and Specialty Center, Austin, TX, United States, [4] Department of Industrial Engineering, Università di Perugia, Perugia, Italy

Anterior cruciate ligament (ACL) deficiency can result in serious degenerative stifle injuries. Although tibial plateau leveling osteotomy (TPLO) is a common method for the surgical treatment of ACL deficiency, alternative osteotomies, such as a leveling osteotomy based on the center of rotation of angulation (CBLO) are described in the literature. However, whether a CBLO could represent a viable alternative to a TPLO remains to be established. The aim of this study is to compare TPLO and CBLO effectiveness in treating ACL rupture. First, a computational multibody model of a physiological stifle was created using three-dimensional surfaces of a medium-sized canine femur, tibia, fibula and patella. Articular contacts were modeled by means of a formulation describing the contact force as function of the interpenetration between surfaces. Moreover, ligaments were represented by vector forces connecting origin and insertion points. The lengths of the ligaments at rest were optimized simulating the drawer test. The ACL-deficient model was obtained by deactivating the ACL related forces in the optimized physiological one. Then, TPLO and CBLO treatments were virtually performed on the pathological stifle. Finally, the drawer test and a weight-bearing squat movement were performed to compare the treatments effectiveness in terms of tibial anteroposterior translation, patellar ligament force, intra-articular compressive force and quadriceps force. Results from drawer test simulations showed that ACL-deficiency causes an increase of the anterior tibial translation by up to 5.2 mm, while no remarkable differences between CBLO and TPLO were recorded. Overall, squat simulations have demonstrated that both treatments lead to an increase of all considered forces compared to the physiological model. Specifically, CBLO and TPLO produce an increase in compressive forces of 54% and 37%, respectively, at 90° flexion. However, TPLO produces higher compressive forces (up to 16%) with respect to CBLO for wider flexion angles ranging from 135° to 117°. Conversely, TPLO generates lower forces in

patellar ligament and quadriceps muscle, compared to CBLO. In light of the higher intra-articular compressive force over the physiological walking range of flexion, which was observed to result from TPLO in the current study, the use of this technique should be carefully considered.

Keywords: multibody, simulation, TPLO, CBLO, ligaments

INTRODUCTION

The main function of the anterior cruciate ligament (ACL) consists in the stabilization of the stifle joint by limiting the anterior translation of the proximal tibia with respect to the distal femur. The ACL insufficiency is an important orthopedic issue which can occur after acute trauma or, more commonly, it can arise from chronic pathological biomechanical stress and constitutes one of the main causes of lameness in dogs (Wilke et al., 2005; Kim et al., 2008; Raske et al., 2013). Furthermore, in the long term, the resulting stifle instability leads to progressive osteoarthritis and severe meniscal injuries (Pozzi et al., 2006; Boundrieau, 2009; Beer et al., 2018). From a biomechanical point of view, the intra-articular forces acting on the tibial plateau under weight-bearing conditions can be resolved into a compressive force, perpendicular to the plateau, and an anterior-posterior (AP) directed force (tangential force), parallel to the plateau (Slocum and Slocum, 1993). The latter force, not being counteracted by ACL action, is at the origin of excessive anterior tibial translation (i.e., drawer sign) which is the clinical sign of an ACL-deficient stifle. Traditional surgery aimed at restabilizing the joint through different approaches classified as intra- and extra-articular procedures. Intra-articular approaches aim to replace the ACL in its anatomical position, whereas, extra-articular approaches try to reduce the stifle instability by means of soft tissue transposition or by using periarticular wires (Kim et al., 2008). Although these traditional approaches are widely used, they produce variable outcomes especially in the long term. In this context, other surgical techniques based on tibial osteotomies have been developed with the intention of recreating the dynamic stability of the ACL-deficient stifle. These techniques are based on a reduction of the tibial plateau slope, aimed at nullifying the tangential articular force, which is responsible for the out-of-range anterior tibial translation during weight-bearing. Over the past decades, several tibial plateau leveling methods have been proposed (Hildreth et al., 2006). Although most of these methods lead to positive clinical results, to date, the most effective surgical treatment based on tibial osteotomy has not been clearly identified yet. A common method is represented by the TPLO, which was first described in 1993 (Slocum and Slocum, 1993). It consists of a radial osteotomy centered at the intercondylar tubercles of the proximal tibia. Subsequently, a rotation of the proximal segment with respect to the distal one is performed to achieve a post-operative tibial plateau angle (TPA) equal to 5°. Another more recent technique is the CBLO (Raske et al., 2013). According to this method, the radial osteotomy is centered over the CORA point, which is defined as the intersection between the proximal and the diaphyseal tibial axes. Successively, the rotation of the proximal tibial segment aims to align the above mentioned

two axes, thus obtaining a post-operative TPA equal to about 10°. For both these techniques, an internal fixation plate combined with surgical bone screws are required to maintain the modified orientation of the proximal tibial segment (Boero Baroncelli et al., 2013). In this scenario, *in silico* modeling can support comparisons among surgical techniques. Specifically, multibody analysis represents an effective computational approach to predict the biomechanical behavior of articular joints in terms of, for instance, range of motion (Zanetti et al., 2018) as well as intra-articular loads (Renani et al., 2018). When these models include also soft tissue, such as muscles and ligaments, both active and passive forces, respectively, can be estimated under some simplified hypothesis (Guess et al., 2016; Zanetti et al., 2017). In this study, for the first time, a computational multibody approach was used to compare TPLO and CBLO effectiveness in treating ACL deficient stifle. First, a multibody model of a physiological stifle joint was created. Secondly, starting from this model, an ACL insufficiency was reproduced. These two first models were validated on reported *in vivo* experimental data (Korvick et al., 1994; Lopez et al., 2003, 2004). Hence, the TPLO and CBLO surgical procedures were virtually performed. Finally, all four models (physiological, ACL-deficient, TPLO-treated, and CBLO-treated) were compared to assess the effectiveness of different treatments, with reference to two loading conditions, specifically, the drawer test and the weight-bearing squat movement. Results pertaining to AP tibial translation and articular forces (i.e., compressive force, quadriceps force, patellar ligament force) were obtained and discussed. We hypothesize that both considered surgical procedures will lead to an increase of the articular forces with respect to the physiological condition.

MATERIALS AND METHODS

In this study, an *in silico* analysis was performed with the objective of comparing the effectiveness of two alternative surgical techniques aimed at treating canine ACL rupture by means of tibial osteotomies. The analysis was carried out using a multibody approach. Initially, the model of a physiological stifle was developed. Subsequently, a pathological (ACL-deficient) model was obtained from the physiological one and both considered surgical techniques (TPLO and CBLO) were virtually performed, resulting in two additional models. Finally, four stifle models were created and subjected to the same tests, namely, the drawer test, focusing on the AP tibial translation, and the weight-bearing squat movement from which results pertaining to AP tibial translation, compressive articular force, quadriceps force, patellar ligament force and angle between the direction of the quadriceps force and the direction of the patellar

ligament were assessed. With reference to the computational model implementation, it should be underlined that (1) contact forces, (2) main muscle forces, and (3) ligaments forces were considered in order to obtain reliable intra-articular forces.

Model Geometry

In this study, four numerical stifle models were created: physiological, pathological (ACL-deficient), TPLO-treated and CBLO-treated. The physiological model was composed by the following bones: femur, tibia, fibula and patella (**Figure 1A**). Bone geometries were obtained from a commercially available CAD model of a medium-sized canine stifle (Sawbones® Europe AB, Malmoe, Sweden). The tibia together with the fibula were modeled as a single body (i.e., tibiofibular joints are considered as fixed joints). The patella was represented as an ellipsoid with its major length based on values found in the literature (Łojszczyk-Szczepaniak et al., 2017) and its other two perpendicular dimensions were chosen to make it congruent to the femoral groove. Given the patellar length, its vertical position with respect to other bones, on the sagittal plane, was chosen based on the mean ratio of the patellar ligament length to the patellar length itself, which is equal to 1.45 (Johnson et al., 2006). The tibial plateau was represented by means of a flat plane with width and length equal to 36 and 23 mm, respectively. An average bone density of 1,800 kg/m³ was assumed and assigned to each bone (Brown et al., 2013). Physiological and ACL-deficient model geometries are identical. Both TPLO-treated and CBLO-treated models were created by modification of the ACL-deficient model according to the respective surgical procedures. TPLO and CBLO stainless fixation plates were treated as additional rigid bodies

(material density of 7,750 kg/m³) attached to the tibial shaft by a fixed joint. Moreover, proximal and distal tibial fragments, resulting from the surgical treatment, were modeled as a single body. Numerical models were created in the multibody dynamic analysis program ADAMS (2017, MSC Software Corporation, Santa Ana, CA).

Contact Modeling

Deformable contacts were defined between the femoral condyles and the tibial plateau, and between the patella and the femoral groove. Contact force was calculated as a function (Equation 1) of both the penetration depth between bodies and the penetration velocity (Terzini et al., 2018).

$$F_c = K\delta^e + C(\delta, \delta_{\max}, C_{\max})\dot{\delta} \qquad (1)$$

where K is the contact stiffness constant, δ is the penetration depth, e is the non-linear power exponent, $\dot{\delta}$ is the penetration velocity and C is the sigmoid damping function which depends on the penetration depth and is defined by a maximum penetration constant δ_{max} and a maximum damping constant C_{max}. The synovial fluid, together with the cartilage, produces a significant joint lubrication. Therefore, the friction forces between the articular surfaces were neglected. Starting from values reported in the literature (Bertocci et al., 2016), the contact parameters were tuned controlling computational costs and avoiding excessive penetration between articular surfaces. **Table 1** reports the final values used for contacts implementation.
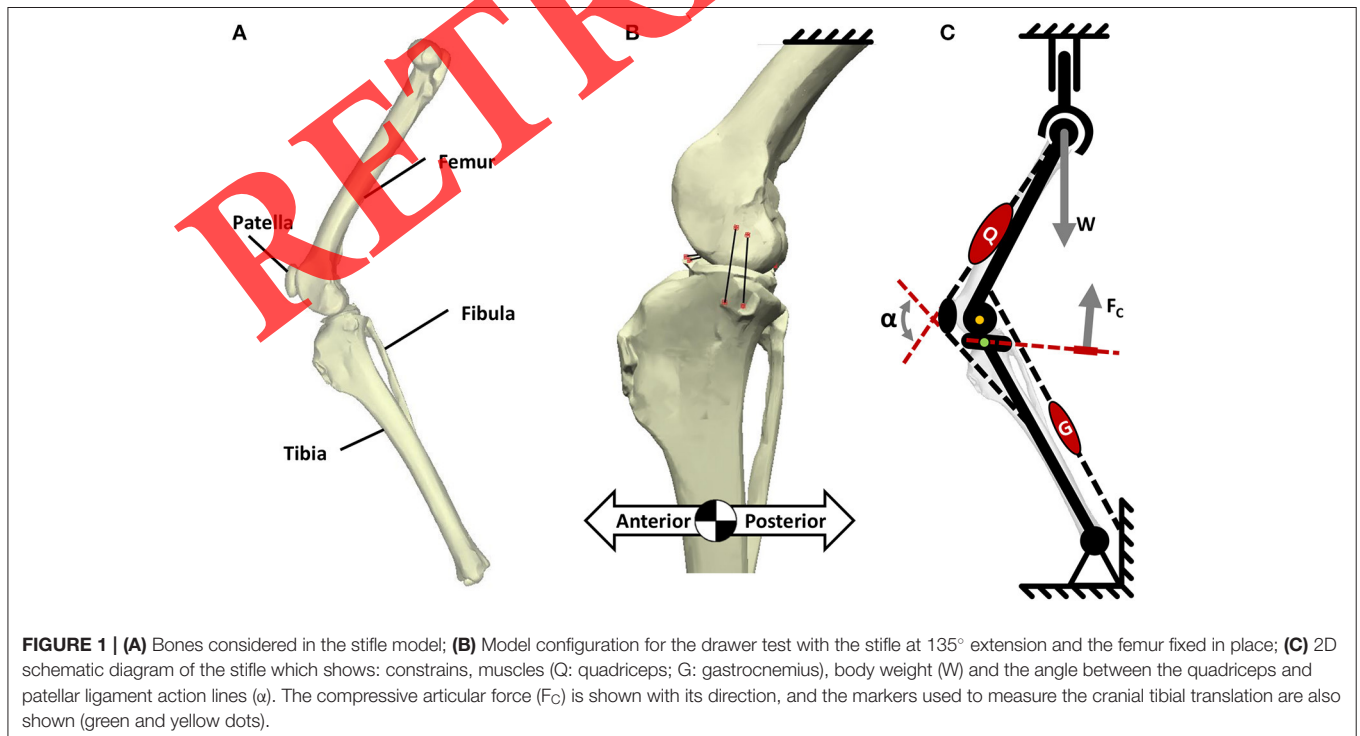

FIGURE 1 | (A) Bones considered in the stifle model; (B) Model configuration for the drawer test with the stifle at 135° extension and the femur fixed in place; (C) 2D schematic diagram of the stifle which shows: constrains, muscles (Q: quadriceps; G: gastrocnemius), body weight (W) and the angle between the quadriceps and patellar ligament action lines (α). The compressive articular force (F_C) is shown with its direction, and the markers used to measure the cranial tibial translation are also shown (green and yellow dots).

TABLE 1 | Value of contact stiffness (K), the non-linear power exponent (e), maximum damping constant (C_{max}), maximum penetration constant (δ_{max}).

Parameter	Value
Stiffness (K)	1,000 N/mm$^{1.5}$
Max damping (C_{max})	1 Ns/mm
Max penetration (δ_{max})	0.01 mm
Power exponent (e)	1.5

Muscles Modeling

The quadriceps muscle and the gastrocnemius were included into the models. Each muscle was represented using a single vector force. The quadriceps muscle was connected at the upper side of the patella. A single insertion point for the gastrocnemius was chosen just above the intercondylar fossa at the midpoint between the rear surfaces of the medial and lateral epicondyle of the femur. During the weight-bearing squat simulation, both quadriceps and gastrocnemius muscles act as traction forces, which avoid the joint collapse by counterbalancing the upper body weight. A proportional-integral-derivative (PID) controller was integrated into the multibody models to simulate muscles action (Fitzpatrick et al., 2012; Stylianou et al., 2013). The vertical position of the femoral head was measured at each time-step analysis and compared to a target vertical position. In the PID controller framework, the measured vertical position of the femoral head represents the input value $y(t)$, whereas the target vertical position represents the setpoint value $Y(t)$. Therefore, the PID controller continuously calculates an error value $e(t)$ as the difference between the setpoint $Y(t)$ and the measured vertical position $y(t)$, and it applies a correction aimed at minimizing this error over time by adjustments of the output $u(t)$, namely, the quadriceps muscle force. The gastrocnemius force is derived from this value, according to a scaling factor, equal to the ratio between the respective physiologic cross-sectional areas (PCSA). For example, this scaling factor results equal to 0.61 for a quadriceps PCSA of 70.5 cm^2 and a gastrocnemius PCSA of 43.0 cm^2 (Williams et al., 2008). A time-dependent setpoint value for the PID controller was used to obtain the weight-bearing squat movement. At the beginning, the setpoint value remains stable so that the physiological stance angle of 135° can be reached. In the following steps, this value decreases over time generating the desired stifle flexion. The PID controller needs to be tuned in order to achieve the best control behavior, by refining the value of K gains which figurate in the proportional, integral, and derivative terms of the PID output $u(t)$. The PID formulation is shown in Equation (2).

$$u(t) = K_p\, e(t) + K_i \int_0^t e(\tau)\, d\tau + K_d \frac{d\,e(t)}{dt} \quad (2)$$

The Ziegler-Nichols tuning method (Ziegler and Nichols, 1995) was chosen to calculate the K gains. This method requires to set the integral (K_i) and derivative (K_d) gains to zero. Then, the proportional gain K_p is increased from zero until it reaches the ultimate gain K_U at which the controller shows stable oscillations.

The ultimate gain K_U and the measured oscillation period P_U are used to set the K_p, K_i and K_d gains by multiplying for predefined constants. In details, $K_p = 0.2 \cdot K_U$, $K_i = 0.2 \cdot K_U \cdot (2/P_U)$, $K_d = 0.2 \cdot K_U \cdot (P_U/3)$. Taking into account the standing configuration, in the presence of the gravitational field, with a body mass of 4.75 kg, then the PID controller output $u(t)$ showed an oscillation period P_U equal to about 0.1 s with an ultimate gain K_U equal to 1,500. Therefore, the following values were obtained: $K_p = 300$ N, $K_i = 6,000$ N/s, $K_d = 10$ Ns. The same values for K gains were used for all simulations.

Ligament Modeling

The following ligaments were included in the physiological model: anterior cruciate ligament (ACL), posterior cruciate ligament (PCL), lateral collateral ligament (LCL), medial collateral ligament (MCL), patellar ligament (PL), medial femoropatellar ligament (MFPL), and lateral femoropatellar ligament (LFPL).

The ACL, PCL, LCL, and MCL were split into two bundles, in detail: MCL anterior (aMCL) and posterior (pMCL) bundle; ACL anteromedial (aACL) and posterolateral (pACL) bundle; PCL anterolateral (aPCL) and posteromedial (pPCL) bundle. This allows considering the ligament structure in bundles with their different constraining contribution. In **Figure 2** are represented the attachment points positions and the bundles orientations of each ligament. In ACL-deficient, TPLO-treated and CBLO-treated models, the ACL ligament was excluded. Each ligament bundle was represented by a single tension-only spring element connecting origin and insertion points that were determined from anatomical references (Carpenter and Cooper, 2000). The non-linear force-strain relationship of each spring was described by the following piecewise function (Equation 3):

$$f = \begin{cases} -k(\varepsilon - \varepsilon_L), & \varepsilon > 2\varepsilon_L \\ -0.25\, k \frac{\varepsilon^2}{\varepsilon_L}, & 0 \leq \varepsilon \leq 2\varepsilon_L \\ 0, & \varepsilon < 0 \end{cases} \quad (3)$$

where ε is the ligament strain, ε_L is a reference value of strain assumed to be 0.03 (Blankevoort et al., 1991) and k is the stiffness parameter, expressed as force per unit strain, of each different ligament bundle. The ligament strain was obtained by considering the zero-load length l_0 that is the maximum linear distance between the ligament attachment points above which the ligament gets taut. The ligament strain ε is defined as Equation (4).

$$\varepsilon = \frac{(l - l_0)}{l_0} \quad (4)$$

All k stiffness parameters are listed in **Table 2** (Brown et al., 2013). The patellar ligament was assumed to act as an inextensible element and, therefore, it was provided with a stiffness value significantly higher than all other ligaments (Haut et al., 1992). In cases of split ligaments, bundles were treated as parallel springs, and the reference stiffness value obtained from literature was equally divided between the springs. With the study focusing on the conditions during the immediate post-operative period only, the viscoelastic behavior of the ligaments, which may affect
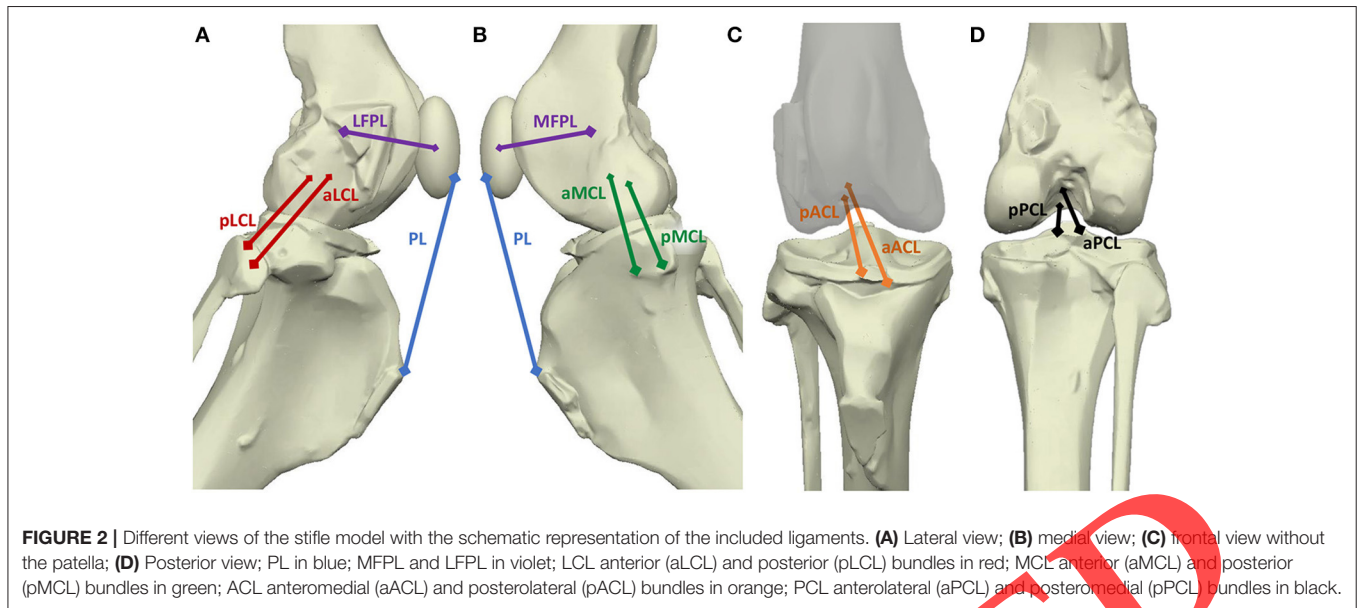
FIGURE 2 | Different views of the stifle model with the schematic representation of the included ligaments. **(A)** Lateral view; **(B)** medial view; **(C)** frontal view without the patella; **(D)** Posterior view; PL in blue; MFPL and LFPL in violet; LCL anterior (aLCL) and posterior (pLCL) bundles in red; MCL anterior (aMCL) and posterior (pMCL) bundles in green; ACL anteromedial (aACL) and posterolateral (pACL) bundles in orange; PCL anterolateral (aPCL) and posteromedial (pPCL) bundles in black.

TABLE 2 | Stiffness parameters (expressed as force per unit strain) for each ligament bundle.

Ligament bundle	k (N)
aACL	3,010
pACL	3,010
aPCL	4,460
pPCL	4,460
aLCL	2,280
pLCL	2,280
aMCL	3,445
pMCL	3,445
PL	11,200
MFPL	2,800
LFPL	2,800

the long-term joint readjustment, was neglected. Nevertheless, in order to avoid high frequency vibrations during simulations, each spring element also included a parallel damper with a damping coefficient of 0.5 Ns/mm.

Ligaments Zero-Load Length Definition

The zero-load length l_0 was determined for each ligament bundle throughout a series of preliminary simulations. First, all bone segments were positioned at 135° extension so that articular surfaces matched, according to anatomical references. The femur was kept fixed in space as well as the patella in the femoral groove, while the tibia-fibula complex was constrained to maintain the 135° extension on the sagittal plane. Muscles, cruciate and collateral ligaments were deactivated at this stage. The static equilibrium conditions of the model were calculated by applying a 10 N upward force, at the tibia center of mass (COM). Zero-load lengths were determined in this configuration as the straight-line
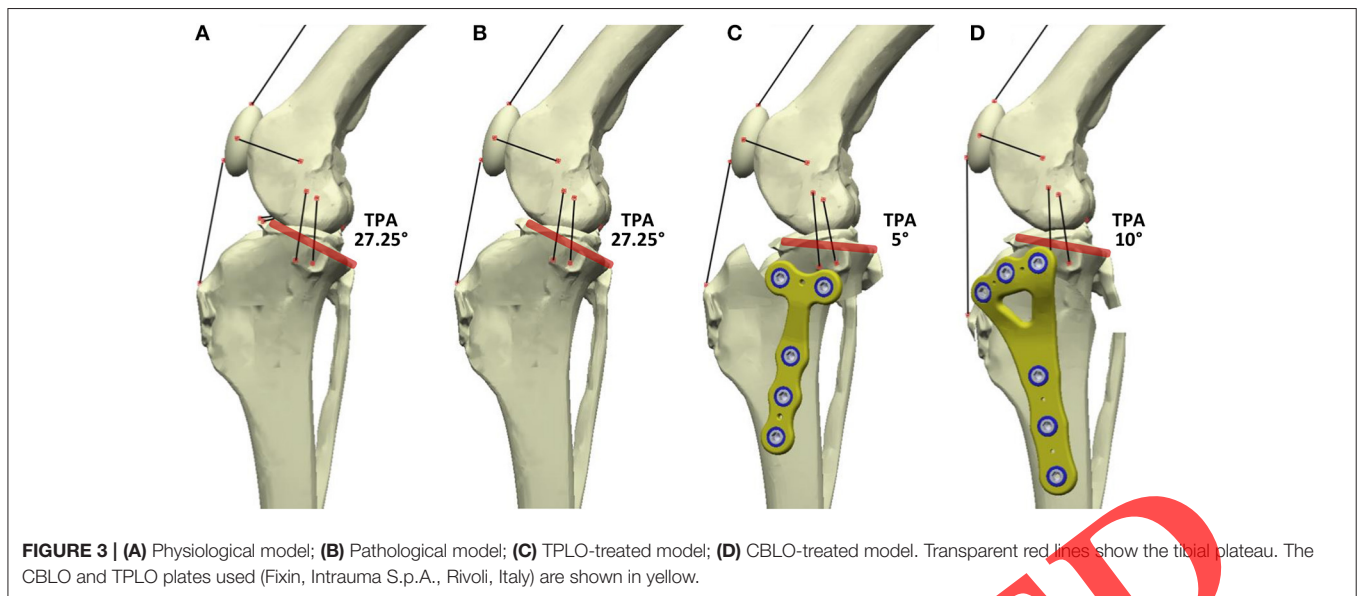
distances between origin and insertion points of each ligament. Successively, cruciate and collateral ligaments were activated and the previously obtained zero-load lengths (initial lengths) were iteratively refined performing the drawer test simulation [see paragraph Model Validation Through Anteroposterior (AP) Drawer Test Simulations], on both physiological and ACL-deficient models, in order to fit AP tibial translations reported in experimental outcomes (Korvick et al., 1994; Lopez et al., 2003, 2004). It is important to note that the so found zero-load lengths (final lengths) were kept constant for all considered models.

Menisci Modeling

The meniscal contribution to the joint dynamics was also taken into account in this study. Specifically, only the constraining forces due to the menisci were simulated (Kang et al., 2017). Therefore, details of the meniscal geometry and femoro-meniscal as well as tibial-meniscal contact forces were neglected. The mechanics of each meniscus (medial and lateral) were represented by two perpendicular springs, acting on the tibial plateau in the anteroposterior and mediolateral directions, respectively. Each spring was constrained at one end on the tibial plateau and at the other end to the femoral condyle. The stiffness of these springs was set equal to 10% the values reported for human menisci that are 5 and 7 N/mm for the AP and mediolateral direction, respectively (Li et al., 1999).

Surgical Procedures

First, the pre-operative TPA was defined by measuring the angle formed between the slope of the medial tibial condyle and the perpendicular to the diaphyseal tibial axis that is, in turn, defined as the line passing through the middle point between the anterior and posterior cortex at the distal 50% and 75% of the tibial shaft length (Osmond et al., 2006). The analyzed tibial geometry presented a pre-operative TPA equal to 27.25° (**Figure 3A**). The TPLO was performed starting from the pathological model of the

FIGURE 3 | (A) Physiological model; **(B)** Pathological model; **(C)** TPLO-treated model; **(D)** CBLO-treated model. Transparent red lines show the tibial plateau. The CBLO and TPLO plates used (Fixin, Intrauma S.p.A., Rivoli, Italy) are shown in yellow.

canine stifle (**Figure 3B**). The TPLO involves the rotation of the proximal tibia to achieve a suggested post-operative TPA of 5° (**Figure 3C**). A circular cut is created in the proximal tibia and then the bone fragment is rotated until the tibial plateau reaches the desired angle. In this study, a 24 mm radius was chosen to produce the cut that was centered over the intercondylar tubercles to maintain enough bone in the proximal segment for an adequate fixation (Kim et al., 2008). Finally, the two portions of the osteotomy are held in position with a TPLO plate. The CBLO was performed starting from the pathological model of the canine stifle, as well. The position of the CORA is located at the intersection between the proximal tibial axis and the diaphyseal tibial axis where the former is obtained as a line passing through the intercondylar tubercles having a posterior angle of 80° from the tibial plateau plane. The osteotomy was centered slightly cranially with respect to the CORA. The exact distance of the osteotomy center from the CORA point was calculated according to the surgical procedure (Raske et al., 2013) and resulted to be equal to 7 mm. The CORA angle is defined as the angle between the proximal tibial axis and the diaphyseal tibial axis. The osteotomy radius was set equal to 18 mm, according to surgical directives that recommend a cut diameter slightly larger than the diameter of the tibial transversal section at the CORA. This surgical procedure aims to reach a post-operative TPA ranging between 9° and 12°, through the alignment of the proximal and diaphyseal tibial axes, that is, setting the CORA angle equal to 0°. In this study, the post-operative TPA has resulted to be equal to 10° (**Figure 3D**). Finally, the two portions of the osteotomy are kept in position by CBLO plate.

Model Validation Through Anteroposterior (AP) Drawer Test Simulations

Drawer test simulation was performed with a dual aim: firstly, it was used to validate the physiological and pathological models by comparison with data from previously reported *in vivo*

experiments (Korvick et al., 1994; Lopez et al., 2003, 2004); secondly, it was used to assess the effect of the two alternative surgical treatments. No muscle activation is supposed to take place during the drawer test simulation; therefore muscles were deactivated for this simulation as well as the patella and its related ligaments (PL, MPFL, and LPFL), since their exclusive function is transferring the quadriceps traction force to the tibial bone segment. The ACL was active only in the physiological case. The hind limb was fixed by fully constraining the femur (**Figure 1B**). At the beginning of the simulation, the tibia-fibula complex was forced to maintain a 135° extension angle. Once the equilibrium was reached, one more constrain was added, forcing the tibia-fibula complex to move on the sagittal plane. The drawer test was performed applying a forward/backward force at the tibia COM. In detail, the force trend over time was defined by a smooth step function (i.e., polynomial Heaviside step function approximation), which increases up to 40 N or decreases up to −40 N (at a rate of about 2.1 N/s) to obtain the anterior or posterior drawer, respectively. During the drawer test, the AP tibial translation was measured as the displacement of the tibial COM along the direction perpendicular to the tibial longitudinal axes. This measure is referred to the equilibrium position, that is, the position that the stifle assumes at the beginning of the simulation when the drawer force has not been applied yet. Then, the measured AP tibial translations were compared with data from previously reported *in vivo* experiments (Korvick et al., 1994; Lopez et al., 2003, 2004).

Squat Simulation

To reproduce *in vivo* four-legged stance condition during weight-bearing squat movement, the gravitational field was included in the model and applied along the vertical direction. The upper end of the hind limb was constrained to a spherical joint, whose center was coincident with the femoral head center. This joint was left free to translate along the vertical direction (**Figure 1C**)

as a result, the femoral head moved along a vertical axis during the squat movement. The limb was constrained to the ground through a revolute joint, at its lower end. This joint was located at the center of the medial malleolus and its axis of rotation was set perpendicular to the sagittal plane. The body mass acting on the limb was located at the upper joint center and it was set equal to 10 kg, which corresponds to 30% of the average body weight of a middle size dog (Kim et al., 2009). The squat movement was obtained through the PID controller which generates the muscle force required to perform the stifle flexion. Hence, the model was free to determine its own kinematics during the simulation. The AP tibial translation during squat simulation was measured as the projection on the tibial plateau of the line connecting two markers, one on the femur and the other one on the tibia. In detail, the femur marker is located at the center of the sphere inscribing the medial femoral condyle, whereas, the tibial marker is located on the tibial plateau at the center of the medial condyle (**Figure 1C**). The AP tibial translation results to be positive or negative when the tibial marker lies anteriorly or posteriorly with respect to the femoral marker, respectively. In particular, squat simulation focused on the assessment of the AP tibial translation, the compressive articular force, the generated quadriceps force as well as the patellar ligament force. Moreover, the angle α defined between the projections on the sagittal plane of the quadriceps line of action and of the patellar ligament line of action (**Figure 1C**) was measured at the beginning (135°) and at the end (90°) of the flexion movement.

RESULTS

The ligaments refinement led to an average variation of about 6.8% of the initial zero-load lengths (**Table 3**).

Findings related to the drawer test simulation revealed that ACL-deficiency causes an increase of the anterior tibial translation, that is, from 1.1 to 6.3 mm (**Figure 4**). Total AP translations equal to 2.3 mm and to 7.5 mm were found for the physiological model and the pathological one, respectively. After surgical treatments, the anterior tibial translation, caused by ACL-deficiency, undergoes a reduction of about 1.5 mm at

the expense of the posterior translation, which increases. Overall, no appreciable differences between CBLO-treated model and TPLO-treated model are evident from the drawer test.

Initial and final stifle configurations obtained from squat simulations are depicted in **Figure 5**. In details, ACL-deficiency resulted in anterior tibial translation of 5.6 mm at 135° (**Figure 6**). Conversely, at the same extension angle, a posterior tibial translation equal to 1.2 mm or even equal to 4.8 mm take place in CBLO- and TPLO-treated model, respectively. In addition, the initial anterior tibial translation in the pathological model is almost completely recovered over the entire flexion arch, reaching a value equal to 1.1 mm at the flexion end. Vice versa, the initial posterior tibial translation in the CBLO-treated model increases over the full flexion range, reaching a value equal to 4.8 mm at 90°. As regards the TPLO-treated model, the initial posterior tibial translation is essentially maintained constant over the whole flexion range, increasing from 4.8 mm to a maximum value equal to 5.6 mm.

The traction force generated by the quadriceps muscle changes considerably among the four models (**Figure 7**). The quadriceps force computed at 135° is about 165 N for all models except for the CBLO, which presents a higher force equal to 196 N. In detail, the muscle forces in the TPLO-treated model and the physiological one are coincident for flexion angles ranging between 135° to about 105°. However, for smaller flexion angle, the muscle force increases faster for the TPLO-treated model compared to the physiological one. Overall, the highest quadriceps force, equal to 973 N, was found for the CBLO-treated model. Similarly to the quadriceps force trends, the highest patellar reaction force was found in the CBLO-treated model (**Figure 8**).

In all cases, the angle α decreases along with the flexion angle (**Table 4**). However, with respect to the physiological model, the pathological condition leads to an increase of the angle equal to 4.7% and 1.4% at 135° and 90° flexion, respectively. On the other hand, a reversed trend results from both TPLO and CBLO

TABLE 3 | Initial and final zero-load lengths (l$_0$) for each ligament bundle.

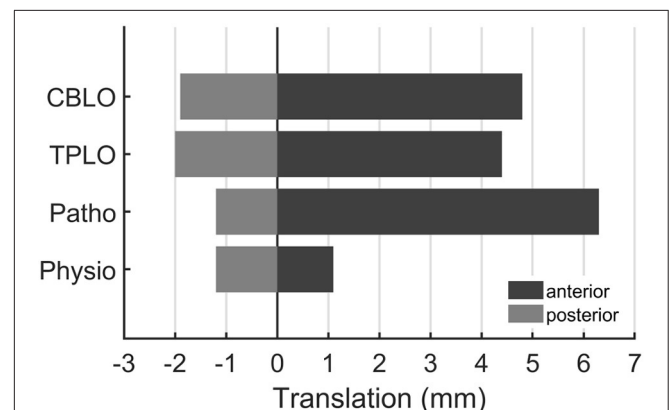| Ligament bundle	Initial l$_0$ (mm)	Final l$_0$ (mm)	Length change (%)
aACL	24.7	26.9	+8.9
pACL	20.7	23.4	+13.0
aPCL	8.3	9.1	+9.6
pPCL	9.4	10.3	+9.6
aLCL	23.6	20.8	−11.9
pLCL	19.7	16.5	−16.2
aMCL	20.7	20.1	−2.9
pMCL	19.2	18.6	−3.1
PL	38.1	38.1	0
MFPL	22.3	22.3	0
LFPL	24.1	24.1	0

FIGURE 4 | Anterior and posterior translations of the tibia relative to the femur, resulting from the drawer test simulation, performed on all models: CBLO-treated (CBLO), TPLO-treated (TPLO), Pathological (Patho), and Physiological (Physio). The vertical zero line is the equilibrium position reached by each model before the application of the AP drawer force.
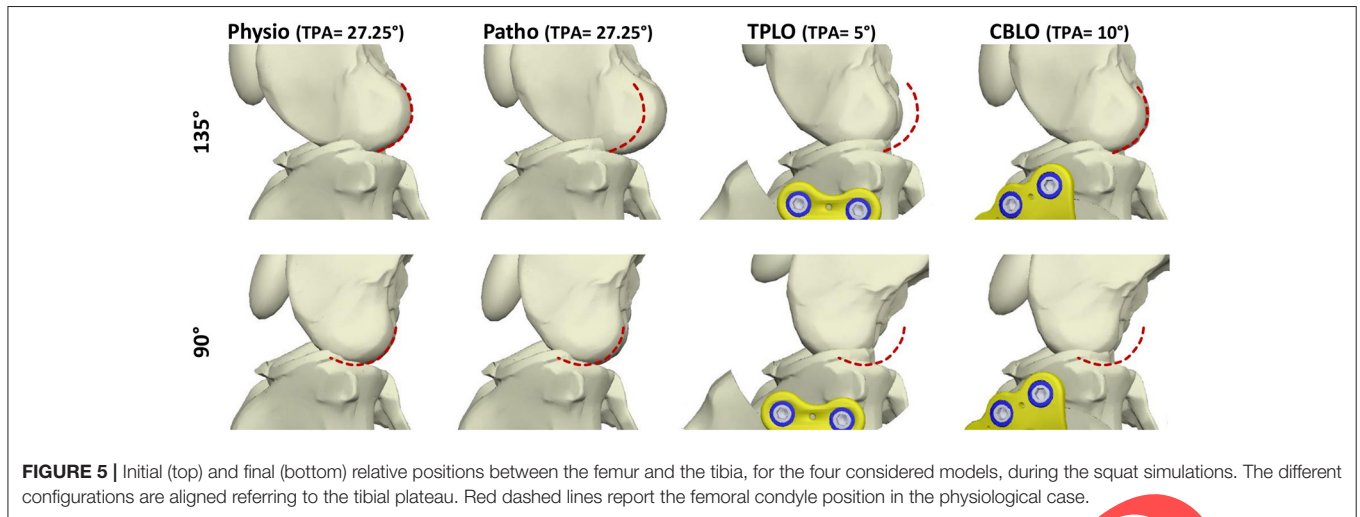
FIGURE 5 | Initial (top) and final (bottom) relative positions between the femur and the tibia, for the four considered models, during the squat simulations. The different configurations are aligned referring to the tibial plateau. Red dashed lines report the femoral condyle position in the physiological case.
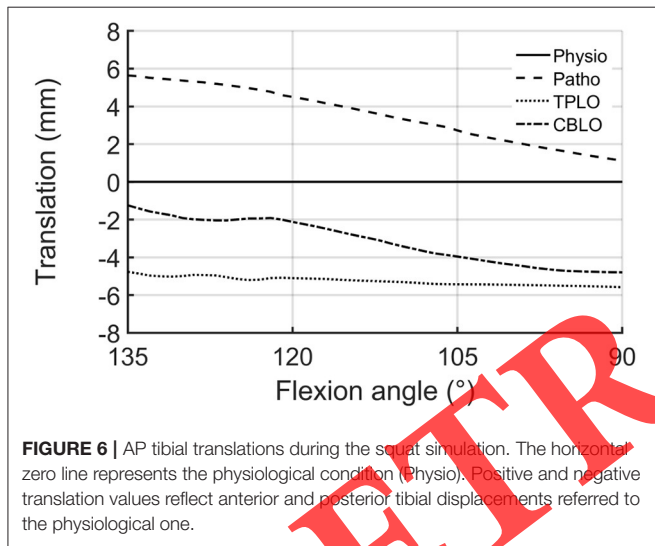

FIGURE 6 | AP tibial translations during the squat simulation. The horizontal zero line represents the physiological condition (Physio). Positive and negative translation values reflect anterior and posterior tibial displacements referred to the physiological one.
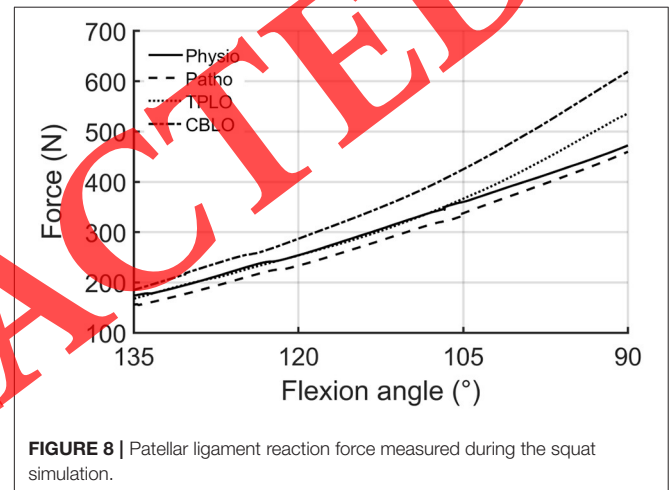

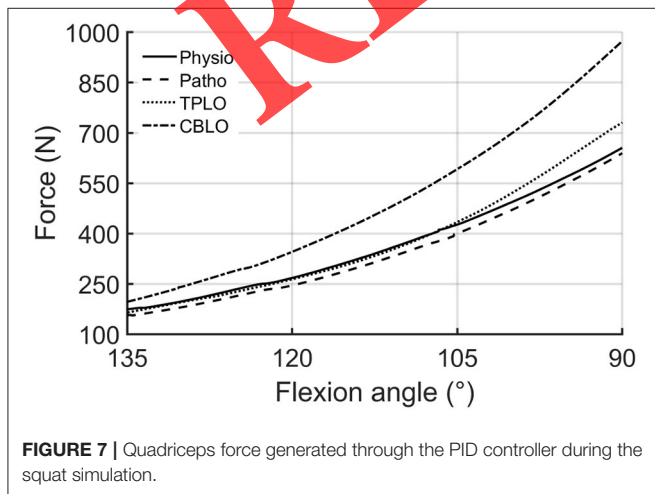**FIGURE 8 |** Patellar ligament reaction force measured during the squat simulation.

TABLE 4 | Variation of the angle α, defined between the quadriceps line of action and the patellar ligament line of action, measured at the beginning (135°) and at the end (90°) of the flexion movement among the four models.

Model	Flexion angle	
	135°	**90°**
Physiological	170°	138°
Pathological	178° (+4.7%)	140° (+1.4%)
TPLO	163° (−4.1%)	130° (−5.8%)
CBLO	155° (−8.8%)	121° (−12.3%)

Percentage of angle variation with respect to the physiological model are reported in brackets.

FIGURE 7 | Quadriceps force generated through the PID controller during the squat simulation.

models, where a narrower angle occurs and decreases over the flexion range, from −4.1% up to −5.8% for the TPLO and from −8.8% up to even −12.3% for the CBLO.

With regard to the compressive articular force, the maximum value took place at 90° flexion angle and was equal to 1,530
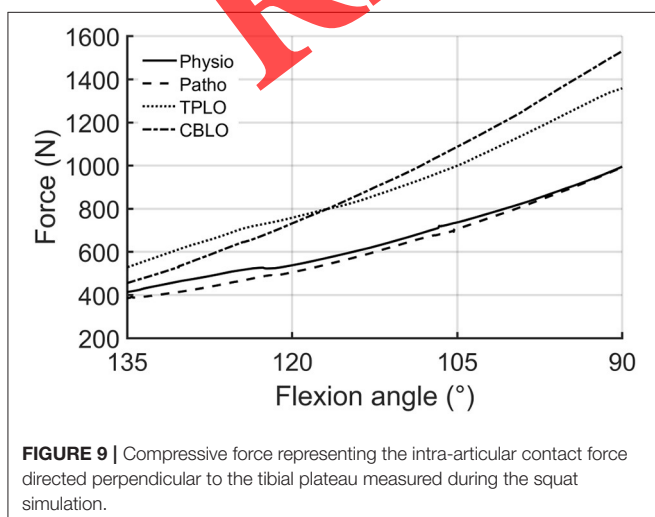
and 1,359 N for the CBLO and the TPLO, respectively, against a value equal to 995 N measured in the physiological model (**Figure 9**). In addition, the CBLO-treated model is affected by a higher increasing rate of the compressive force compared to the TPLO-treated one. As a result, the CBLO produces a lower force compared to the TPLO for flexion angles ranging from 135° to 117°.

DISCUSSION

In this study, a computational multibody analysis was performed with the aim to compare TPLO and CBLO effectiveness in treating ACL deficiency under the hypothesis that both considered surgical procedures induce an increase of the articular forces with respect to the physiological condition.

The drawer test simulation confirmed that the absence of the ACL constraining force causes an increase of the anterior tibial translation. Although several studies have reported the effect of ACL rupture on tibial translation, a direct comparison of these findings was difficult due to variations in tests across studies. Nevertheless, the translational values obtained from the drawer test in this study are consistent with *in vivo* experimental data reported by Lopez et al. (2003, 2004) and Korvick et al. (1994) for pathological and physiological conditions. In addition, our results show that both treatments produce only a slight reduction of the total AP tibial translation compared to the pathological model. This was expected since both treatments aim to achieve a dynamic stabilization of the joint in a weight-bearing condition, that is, when the body weight and the muscle actions give an additional contribution to the joint stability. In the drawer test, the only stabilizing action is played by stretched ligaments; hence, the TPA modification has a minimal impact on the total AP translation due to tibiofemoral articular surfaces reciprocal sliding, according to the tibial slope.

As far as the squat flexion is concerned, both surgical treatments generate an inversion in the tibial translation, namely, the tibia move posteriorly with respect to the physiological condition. This same inversion was reported in TPLO-treated stifles in the experimental study by Warzee et al. (2001).

FIGURE 9 | Compressive force representing the intra-articular contact force directed perpendicular to the tibial plateau measured during the squat simulation.

Furthermore, important considerations can be drawn from an analysis of the traction force generated by the quadriceps muscle. In general, the minimum computed forces for quadriceps are lower than those reported by other experimental studies (Drew et al., 2018; Kanno et al., 2019), where, however, the application method of the emulated muscle forces is not well-defined. The highest quadriceps force was found in the CBLO-treated model. This is likely to be due to the anterior translation of the femoral condyles that results in a reduction of the quadriceps moment arm (Grelsamer and Klein, 1998; Schindler and Scott, 2011; Kanno et al., 2019). Therefore, a higher muscle force is needed to obtain a given joint extension moment.

In addition, the angle α between the direction of the quadriceps force and the direction of the patellar ligament also plays an influence (Aglietti and Menchetti, 1995). Specifically, a lower value of this angle entails higher quadriceps forces. The lowest angle was found for the CBLO-treated model, giving a contribution to the quadriceps force increase.

The pattern of the patellar ligament force is similar to that of the quadriceps force, since these quantities are closely related, so the higher patellar forces are produced by the CBLO procedure. On that note, it should be reminded that higher patellar ligament forces mean higher ligament stresses which, in turn, may lead to ligament thickening or desmitis (Mattern et al., 2006; Milovancev and Schaefer, 2009; Beer et al., 2018).

Overall, the basic concept behind TPLO surgery is converting tangential forces acting on the tibial plateau into a compressive reaction force, normal to the plateau itself (Slocum and Slocum, 1993). However, an excessive compressive force could lead to degenerative complications, such as osteoarthritis and meniscal injuries (Beer et al., 2018). From articular compressive forces computed during squat simulations, it is evident how the ACL-deficient stifle undergoes a lower compressive articular force, compared to the physiological stifle, and this is in accordance with Kim et al. (2009). In contrast, both surgical treatments cause an increase of this compressive force. As known, surgery for ACL-deficiency is performed on pathologic stifles characterized by degenerated cartilage. Therefore, the higher articular compressive force in limb extension, following TPLO, should be reason for concern regarding this technique.

As a matter of fact, this study is affected by some limitations which should be highlighted. First, it should be taken into account that the physiological and pathological models were validated solely on AP tibial translations resulting from previous *in vivo* experiments involving the drawer test. Another limit was the estimation of the gastrocnemius contribution as a fraction of the quadriceps action. Moreover, the present study was addressed to a short-time post-operative scenario, hence, neglecting phenomena that might occur over time due to soft tissue behaviors (e.g., stress-relaxation and recovery phenomena).

SUMMARY AND CONCLUSION

To date, no study has investigated the effectiveness of CBLO compared to TPLO. In this study, a first comparative analysis was performed by means of a computational multibody approach, giving the certainty of equally applied boundary conditions to all

compared models. The presented models confirm the feasibility of this approach in studying stifle biomechanics also when the joint geometry is altered, namely, after surgical treatments that involve osteotomies. Overall, no appreciable differences between CBLO and TPLO emerged from the clinical drawer test. Results from the squat simulations show that both treatments cause an increase in all measured forces (patellar ligament force, compressive force and quadriceps force). However, the TPLO generates lower forces in patellar ligament and quadriceps muscle compared to CBLO. Nevertheless, if compared to TPLO, the CBLO produces a lower compressive force for flexion angles ranging from 135° to about 117°. In conclusion, this work represents the first step toward the development of a complete comparative analysis including also other significant parameters (e.g., the pre- and post-TPA) and other surgical treatments.

DATA AVAILABILITY

The datasets generated for this study are available on request to the corresponding author.

AUTHOR CONTRIBUTIONS

GP and MT have implemented the numerical models and have performed numerical simulations. GP was specifically involved in parameters optimization and data post-processing. BB and DH contributed to the conception of the study, providing particular assistance in clinical considerations. CB, AA, and EZ supervised the work and specifically pointed out biomechanical aspects of the study. AA, in particular, has organized the work defining its objectives. GP wrote the first draft of the manuscript. MT and EZ contributed to manuscript revision.

REFERENCES

Aglietti, P., and Menchetti, P. P. M. (1995). "Biomechanics of the patellofemoral joint," in *The Patella*, ed Giles R. Scuderi (New York, NY: Springer), 25–48. doi: 10.1007/978-1-4612-4188-1_3

Beer, P., Bockstahler, B., and Schnabl-Feichter, E. (2018). Tibial plateau leveling osteotomy and tibial tuberosity advancment–a systematic review. *Tierarztl Prax Ausg K Kleintiere Heimtiere* 46, 223–235. doi: 10.15654/TPK-170486

Bertocci, G. E., Brown, N. P., Embleton, N. A., and Barkowski, V. J. (2016). Canine stifle biomechanics associated with a novel extracapsular articulating implant predicted using a computer model. *Vet. Surg.* 45, 327–335. doi: 10.1111/vsu.12450

Blankevoort, L., Kuiper, J. H., Huiskes, R., and Grootenboer, H. J. (1991). Articular contact in a three-dimensional model of the knee. *J. Biomech.* 24, 1019–1031. doi: 10.1016/0021-9290(91)90019-J

Boero Baroncelli, A., Reif, U., Bignardi, C., and Peirone, B. (2013). Effect of screw insertion torque on push-out and cantilever bending properties of five different angle-stable systems. *Vet. Surg.* 42, 308–315. doi: 10.1111/j.1532-950X.2013.01088.x

Boundrieau, R. J. (2009). Tibial plateau leveling osteotomy or tibial tuberosity advancement? *Vet. Surg.* 38, 1–22. doi: 10.1111/j.1532-950X.2008.00439.x

Brown, N. P., Bertocci, G. E., and Marcellin-Little, D. J. (2013). Development of a canine stifle computer model to evaluate cranial cruciate ligament deficiency. *J. Mech. Med. Biol.* 13:1350043. doi: 10.1142/S0219519413500437

Carpenter, D. H., and Cooper, R. C. (2000). Mini review of canine stifle joint anatomy. *Anat. Histol. Embryol.* 29, 321–329. doi: 10.1046/j.1439-0264.2000.00289.x

Drew, J. O., Glyde, M. R., Hosgood, G. L., and Hayes, A. J. (2018). The efeect of tibial plateau levelling osteotomy on stifle extensor mechanism load: a canine *ex vivo* study. *Vet. Comp. Orthop. Traumatol.* 31, 131–136. doi: 10.1055/s-0038-1627476

Fitzpatrick, C. K., Baldwin, M. A., Clary, C. W., Maletsky, L. P., and Rullkoetter, P. J. (2012). Evaluating knee replacement mechanics during ADL with PID-controlled dynamic finite element analysis. *Comput. Methods Biomech. Biomed. Engin.* 17, 360–369. doi: 10.1080/10255842.2012.684242

Grelsamer, R. P., and Klein, J. R. (1998). The biomechanics of the patellofemoral joint. *J. Orthop. Sport. Phys. Ther.* 28, 286–298. doi: 10.2519/jospt.1998.28.5.286

Guess, T. M., Razu, S., and Jahandar, H. (2016). Evaluation of knee ligament mechanics using computational models. *J. Knee Surg.* 29, 126–137. doi: 10.1055/s-0036-1571954

Haut, R. C., Lancaster, R. L., and DeCamp, C. E. (1992). Mechanical properties of the canine patellar tendon: some correlations with age and the content of collagen. *J. Biomech.* 25, 163–165. doi: 10.1016/0021-9290(92)90273-4

Hildreth, B. E., Marcellin-Little, D. J., Roe, S. C., and Harrysson, O. L. A. (2006). *In vitro* evaluation of five canine tibial plateau leveling methods. *Am. J. Vet. Res.* 67, 693–700. doi: 10.2460/ajvr.67.4.693

Johnson, A. L., Monsere, J., Sepulveda, G., Broaddus, K. D., Hauptman, J. G., and Marsh, S. (2006). Vertical patellar position in large-breed dogs with clinically normal stifles and large-breed dogs with medial patellar luxation. *Vet. Surg.* 35, 78–81. doi: 10.1111/j.1532-950X.2005.00115.x

Kang, K.-T., Koh, Y.-G., Jung, M., Nam, J.-H., Son, J., Lee, Y. H., et al. (2017). The effects of posterior cruciate ligament deficiency on posterolateral corner structures under gait- and squat-loading conditions. *Bone Joint Res.* 6, 31–42. doi: 10.1302/2046-3758.61.BJR-2016-0184.R1

Kanno, N., Ochi, Y., Ichinohe, T., Hakozaki, T., Suzuki, S., Harada, Y., et al. (2019). Effect of the centre of rotation in tibial plateau levelling osteotomy on quadriceps tensile force: an *ex vivo* study in canine cadavers. *Vet. Comp. Orthop. Traumatol.* 32, 117–125. doi: 10.1055/s-0039-1677868

Kim, S. E., Pozzi, A., Banks, S. A., Conrad, B. P., and Lewis, D. D. (2009). Effect of tibial tuberosity advancement on femorotibial contact mechanics and stifle kinematics. *Vet. Surg.* 38, 33–39. doi: 10.1111/j.1532-950X.2008.00471.x

Kim, S. E., Pozzi, A., Kowaleski, M. P., and Lewis, D. D. (2008). Tibial osteotomies for cranial cruciate ligament insufficiency in dogs. *Vet. Surg.* 37, 111–125. doi: 10.1111/j.1532-950X.2007.00361.x

Korvick, D. L., Pijanowski, G. J., and Schaeffer, D. J. (1994). Three-dimensional kinematics of the intact and cranial cruciate ligament-deficient stifle of dogs. *J. Biomech.* 27, 77–87. doi: 10.1016/0021-9290(94)90034-5

Li, G., Gil, J., Kanamori, A., and Woo, S. L.-Y. (1999). A validated three-dimensional computational model of a human knee joint. *J. Biomech. Eng.* 121:657. doi: 10.1115/1.2800871

Łojszczyk-Szczepaniak, A., Silmanowicz, P., Komsta, R., and Osinski, Z. (2017). Determination of reference values and frequency of occurrence of patella alta in German shepherd dogs: a retrospective study. *Acta Vet. Scand.* 59, 1–6. doi: 10.1186/s13028-017-0304-1

Lopez, M. J., Hagquist, W., Jeffrey, S. L., Gilbertson, S., and Markel, M. D. (2004). Instrumented measurement of *in vivo* anterior-posterior translation in the canine knee to assess anterior cruciate integrity. *J. Orthop. Res.* 22, 949–954. doi: 10.1016/j.orthres.2003.10.017

Lopez, M. J., Kunz, D., Vanderby, R. J., Heisey, D., Bogdanske, J., and Markel, M. D. (2003). A comparison of joint stability between anterior cruciate intact and deficient knees: a new canine model of anterior cruciate ligament disruption. *J. Orthop. Res.* 21, 224–230. doi: 10.1016/S0736-0266(02)00132-8

Mattern, K. L., Berry, C. R., Peck, J. N., and Haan, J. J., De. (2006). Radiographic and ultrasonographic evaluation of the patellar ligament following tibial plateau leveling osteotomy. *Vet. Radiol. Ultrasound* 47, 185–191. doi: 10.1111/j.1740-8261.2006.00126.x

Milovancev, M., and Schaefer, S. (2009). Tibial plateau leveling osteotomy. *Adv. Vet. Surg. Canine Cranial Cruciate Ligament* 02115, 169–175. doi: 10.1002/9781118786796.ch25

Osmond, C. S., Marcellin-Little, D. J., Harrysson, O. L. A., and Kidd, L. B. (2006). Morphometric assessment of the proximal portion of the tibia in dogs with and

without cranial cruciate ligament rupture. *Vet. Radiol. Ultrasound* 47, 136–141. doi: 10.1111/j.1740-8261.2006.00119.x

Pozzi, A., Kowaleski, M. P., Apelt, D., Meadows, C., Andrews, C. M., and Johnson, K. A. (2006). Effect of medial meniscal releas on tibial translation after tibial plateau leveling osteotomy. *Vet. Surg.* 35, 486–494. doi: 10.1111/j.1532-950X.2006.00180.x

Raske, M., Hulse, D., Beale, B., Saunders, W. B., Kishi, E., and Kunze, C. (2013). Stabilization of the CORA based leveling osteotomy for treatment of cranial cruciate ligament injury using a bone plate augmented with a headless compression screw. *Vet. Surg.* 42, 759–764. doi: 10.1111/j.1532-950X.2013.12035.x

Renani, M. S., Rahman, M., Cil, A., and Stylianou, A. P. (2018). Calibrating multibody ulno-humeral joint cartilage using a validated finite element model. *Multibody Syst. Dyn.* 44, 81–91. doi: 10.1007/s11044-018-9622-y

Schindler, O. S., and Scott, W. N. (2011). Basic kinematics and biomechanics of the patello-femoral joint part 1: the native patella. *Acta Orthop. Belg.* 77, 421–431.

Slocum, B., and Slocum, T. D. (1993). Tibial plateau leveling osteotomy for repair of cranial cruciate ligament rupture in the canine. *Vet. Clin. North Am. Small Anim. Pract.* 23, 777–795. doi: 10.1016/S0195-5616(93)50082-7

Stylianou, A. P., Guess, T. M., and Kia, M. (2013). Multibody muscle driven model of an instrumented prosthetic knee during squat and toe rise motions. *J. Biomech. Eng.* 135:041008. doi: 10.1115/1.4023982

Terzini, M., Zanetti, E. M., Audenino, A. L., Putame, G., Gastaldi, L., Pastorelli, S., et al. (2018). Multibody modelling of ligamentous and bony stabilizers in the human elbow. *Muscle Ligaments Tendons J.* 07:493. doi: 10.32098/mltj.04.2017.03

Warzee, C. C., Dejardin, L. M., Arnoczky, S. P., and Perry, R. L. (2001). Effect of tibial plateau leveling on cranial and caudal tibial thrusts in canine cranial cruciate-deficient stifles: an *in vitro* experimental study. *Vet. Surg.* 30, 278–286. doi: 10.1053/jvet.2001.21400

Wilke, V. L., Robinson, D. A., Evans, R. B., Rothschild, M. F., and Conzemius, M. G. (2005). Estimate of the annual economic impact of treatment of cranial cruciate ligament injury in dogs in the United States. *J Am Vet Med Assoc.* 227, 1604–1607. doi: 10.2460/javma.2005.227.1604

Williams, S. B., Wilson, A. M., Rhodes, L., Andrews, J., and Payne, R. C. (2008). Functional anatomy and muscle moment arms of the pelvic limb of an elite sprinting athlete: the racing greyhound (*Canis Familiaris*). *J. Anat.* 213, 361–372. doi: 10.1111/j.1469-7580.2008.00961.x

Zanetti, E., Terzini, M., Mossa, L., Bignardi, C., Costa, P., Audenino, A., et al. (2017). A structural numerical model for the optimization of double pelvic osteotomy in the early treatment of canine hip dysplasia. *Vet. Comp. Orthop. Traumatol.* 30, 256–264. doi: 10.3415/VCOT-16-05-0065

Zanetti, E. M., Bignardi, C., Terzini, M., Putame, G., and Audenino, A. L. (2018). A multibody model for the optimization of hip arthroplasty in relation to range of movement. *Australas. Med. J.* 11, 486–491. doi: 10.21767/AMJ.2018.3444

Ziegler, J. G., and Nichols, N. B. (1995). Optimum settings for automatic controllers. *InTech* 42, 94–100. doi: 10.1115/1.2899060